2014

Synthesis and Spectroscopic Characterization of High-Spin Mononuclear Iron(II) p-Semiquinonate Complexes

Amanda E. Baum
Marquette University, amanda.baum@marquette.edu

Heaweon Park
Marquette University

Sergey V. Lindeman
Marquette University, sergey.lindeman@marquette.edu

Adam T. Fiedler
Marquette University, adam.fiedler@marquette.edu

Inorganic Chemistry

Communication

pubs.acs.org/IC

Synthesis and Spectroscopic Characterization of High-Spin Mononuclear Iron(II) *p*-Semiquinonate Complexes

Amanda E. Baum, Heaweon Park, Sergey V. Lindeman, and Adam T. Fiedler*

Department of Chemistry, Marquette University, 535 North 14th Street, Milwaukee, Wisconsin 53233, United States

Supporting Information

ABSTRACT: Two mononuclear iron(II) *p*-semiquinonate (*p*SQ) complexes have been generated via one-electron reduction of precursor complexes containing a substituted 1,4-naphthoquinone ligand. Detailed spectroscopic and computational analysis confirmed the presence of a coordinated *p*SQ radical ferromagnetically coupled to the high-spin Fe^{II} center. The complexes are intended to model electronic interactions between (semi)quinone and iron cofactors in biology.

Substituted *p*-quinones are common redox-active molecules that appear in a variety of biological contexts, including respiration, photosynthesis, and enzymatic transformations.[1] These cofactors participate in reversible one- and two-electron reactions that are often coupled to proton transfer(s), yielding the corresponding semiquinone (pSQ$^{\bullet-}$) and hydroquinone (*p*HQ) species, respectively. (Hydro)quinones often function in concert with protein-bound metal ions, including heme and nonheme iron centers. For instance, cytochrome bc_1 (respiratory complex III) catalyzes the two-electron oxidation of the *p*HQ cofactor ubiquinol; the first electron is transferred to an Fe−S (Rieske) cluster and the second to heme b_L.[2] Recent studies with electronic paramagnetic resonance (EPR) spectroscopy have detected the triplet state arising from ferromagnetic interactions between the ubisemiquinone radical and reduced Fe−S cluster.[3] Similarly, a nonheme Fe^{II} center in photosystem II (PSII) is associated with two *p*-quinones that shuttle electrons away from the photoexcited P_{680} cofactor, resulting in short-lived Fe^{II}-*p*SQ$^{\bullet-}$ states than have been detected by EPR.[4] Finally, a superoxo-Fe^{II}-*p*SQ$^{\bullet-}$ intermediate has been proposed in the catalytic cycle of mononuclear nonheme iron enzymes known as hydroquinone dioxygenases,[5] which play an important role in the biodegradation of aromatic pollutants.

Despite these biological precedents, only a handful of synthetic iron complexes with *p*-quinone ligands have been crystallographically characterized, and the majority of these are diiron complexes with a bridging quinone.[6] The dearth of monoiron complexes is likely due to the inability of the *p*-quinone unit to form chelates, combined with the weak donor properties of carbonyls. To the best of our knowledge, there are no prior examples of mononuclear iron complexes featuring *p*SQ$^{\bullet-}$ ligands, although Riordan and co-workers recently generated a five-coordinate iron(II) complex containing a bidentate *o*-semiquinonate ligand.[7]

This paper describes the synthesis and characterization of metastable Fe^{II}-*p*SQ$^{\bullet-}$ complexes with relevance to the transient intermediates found in proteins. Our approach required the initial preparation of two monoiron(II) complexes (**1** and **2**) each containing a juglone-derived ligand (either ^{H}**J**$^{-}$ or ^{Br}**J**$^{-}$; Figure 1a). The presence of the phenolate donor

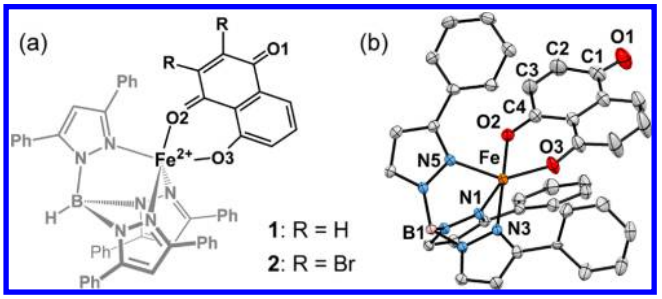

Figure 1. (a) Schematic of complexes **1** and **2**. (b) Thermal ellipsoid diagram of **1**. H atoms and 5-Ph substituents of the ^{Ph2}Tp ligand have been omitted for clarity.

ensures coordination of the 1,4-naphthoquinone moiety via formation of a favorable six-membered ring chelate. The high-spin Fe^{II} center is also bound to the hydrotris(3,5-diphenylpyrazol-1-yl)borate (^{Ph2}Tp) supporting ligand. Significantly, treatment of **1** and **2** with a suitable one-electron reductant yielded brown chromophores (**1**^{red} and **2**^{red}, respectively) that are stable at low temperatures. Extensive analysis with spectroscopic [UV−vis absorption, EPR, and resonance Raman (rR)] and computational methods, described below, confirmed the formation of mononuclear Fe^{II}-*p*SQ$^{\bullet-}$ species, the first to be reported in the literature. Our synthetic efforts thus provide a valuable platform for detailed explorations of iron−(semi)quinone interactions.

Complexes **1** and **2** were prepared by mixing [Fe^{2+}(^{Ph2}Tp)(OBz)] with equimolar amounts of NaOMe and the appropriate juglone (^{H}**JH** or ^{Br}**JH**) in CH_2Cl_2 under anaerobic conditions. X-ray-quality crystals were obtained by layering 1,2-dichloroethane solutions with either MeCN (**1**) or pentane (**2**). In each case, the resulting structure revealed a pentacoordinate Fe^{II} center bound to a facially coordinating ^{Ph2}Tp ligand and bidentate ^{R}**J**$^{-}$ anion (Figure 1b and Table S1 in the Supporting Information, SI). The observed metric parameters (Table S2 in the SI) are quite similar for the two complexes. Both structures feature distorted trigonal-bipyramidal coordination geometries

Received: October 22, 2014
Published: November 13, 2014

   dx.doi.org/10.1021/ic502564r | *Inorg. Chem.* 2014, 53, 12240−12242

(τ values[8] of 0.63) with the phenolate (O3) and carbonyl (O2) donors of $^{R}J^{-}$ in equatorial and axial positions, respectively. The $^{R}J^{-}$ ligand binds in an asymmetric manner, with a short Fe−O3 distance of 1.93 Å and a longer Fe−O2 distance near 2.07 Å. The average Fe−N_{Tp} bond length of ∼2.13 Å is typical of high-spin (S = 2) ferrous complexes,[9] consistent with the magnetic moments of 4.85(10) μ_B. The $^{R}J^{-}$ ligands exhibit short O1−C1 and O2−C4 distances (1.22 and 1.24 ± 0.01 Å, respectively) characteristic of quinone moieties.

Complex **1** possesses a deep-violet color in solution because of the presence of two absorption bands at 510 and 910 nm (ε = 5.3 and 2.0 mM^{-1} cm^{-1}, respectively; see Figure 2, left).

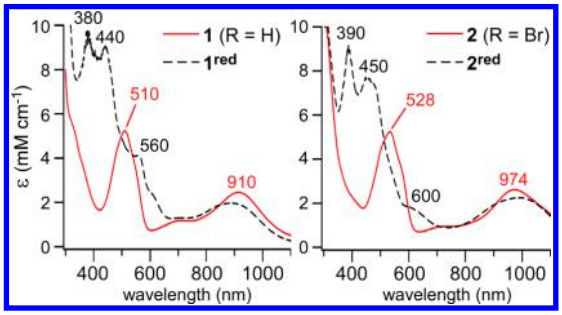

Figure 2. Red, solid lines: UV−vis absorption spectra of **1** and **2** in CH_2Cl_2 at room temperature. Black, dashed lines: Spectra measured after the addition of 1 equiv of $CoCp^*_2$ (**1**) or $CoCp_2$ (**2**) at −30 °C in CH_2Cl_2 to give the corresponding $\mathbf{X}^{red}$ species.

Time-dependent (TD) density functional theory (DFT) calculations attribute the lower-energy band to a $Fe^{II} \rightarrow {}^{H}J^{-}$ metal-to-ligand charge transfer (MLCT) transition, while the higher-energy feature arises from an intraligand $\pi \rightarrow \pi^*$ transition localized on $^{H}J^{-}$ (Figure S1 in the SI). Both transitions red-shift by approximately 700 cm^{-1} in the spectrum of **2** (Figure 2) because of the presence of electron-withdrawing Br substituents.

To assess the feasibility of generating iron(II) semiquinonate species via one-electron reduction, the electrochemical properties of **1** and **2** were examined in CH_2Cl_2 solutions. In each case, cyclic voltammetry (CV) exhibits a semireversible one-electron oxidation near 0.15 V versus $Fc^{+/0}$ (Figure 3), which is

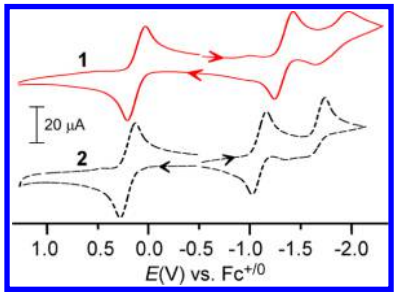

Figure 3. Cyclic voltammograms of **1** and **2** in CH_2Cl_2 with 0.1 M $(NBu_4)PF_6$ as the supporting electrolyte.

assigned to the $Fe^{2+/3+}$ redox couple based on our experience with related complexes.[9] At lower potentials, complex **1** displays a semireversible couple at −1.33 V and an irreversible peak at −1.97 V. A comparison to redox potentials measured for 1,4-naphthoquinone in MeCN (−1.11 and −1.74 V)[10] indicates that these low-potential events arise from successive one-electron reductions of the $^{H}J^{-}$ ligand. The corresponding features in the CV of **2** are shifted to more positive potentials by 0.23 V (Figure 3), reflecting the electron-poor nature of the $^{Br}J^{-}$ ligand.

Having established the redox properties of the iron(II) *p*-quinone complexes, we proceeded to monitor their reactivity with chemical reductants. Guided by the CV data, complex **1** was treated with 1 equiv of $CoCp^*_2$ (E° = −1.94 V in CH_2Cl_2), while the more-easily reduced **2** was treated with $CoCp_2$ (E° = −1.33 V).[11] The addition of these reductants to solutions of **1** and **2** in CH_2Cl_2 instantly generates new chromophores ($\mathbf{1}^{red}$ and $\mathbf{2}^{red}$, respectively) with two intense absorption features in the near-UV region (ε values of 8−10 mM^{-1} cm^{-1}; Figure 2). In addition, each complex displays a shoulder near 600 nm and a broad near-IR feature. These features do not arise from either (decamethyl)cobaltocene or its oxidized derivative (Figure S2 in the SI). The $\mathbf{X}^{red}$ species are stable for several minutes under anaerobic conditions and low temperatures (<−30 °C) but decay rapidly at room temperature to the starting material. The sizable intensities and sharp nature of the near-UV bands suggest that they arise from ligand-based $\pi-\pi^*$ transitions, consistent with transient absorption studies of *p*-semiquinones that detected strong absorption features in the same region.[12] Moreover, the $\mathbf{X}^{red}$ absorption spectra bear close similarities to the one reported for Riordan's Fe^{II}-*o*$SQ^{\bullet-}$ complex.[7]

The X-band EPR spectrum of $\mathbf{2}^{red}$, collected at 20 K in frozen CH_2Cl_2, consists of two $S = {}^{5}/_{2}$ signals, as is evident by the low-field peaks at g = 8.6 and 10.1 in Figure 4. Simulation of the $\mathbf{2}^{red}$

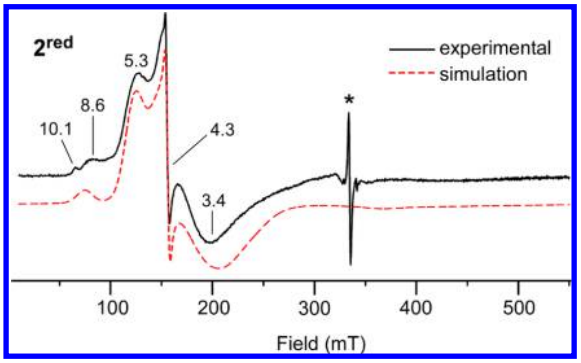

Figure 4. X-band EPR spectrum of $\mathbf{2}^{red}$ in frozen CH_2Cl_2 at 20 K. The sharp feature (*) arises from a radical impurity. Simulation of the data required two $S = {}^{5}/_{2}$ species with the following parameters: major (92%), D = −4.0 cm^{-1}, E/D = 0.18, g = 2.0, 2.0, and 2.1; minor (8%), D = 1.6 cm^{-1}, E/D = 0.33, g_{iso} = 2.0.

data at multiple temperatures (Figure S3 in the SI) determined that the dominant $S = {}^{5}/_{2}$ species, accounting for 92% of the total intensity, has a negative D value and moderate rhombicity (E/D = 0.18). The minor $S = {}^{5}/_{2}$ species is highly rhombic, characteristic of high-spin Fe^{III} ions in low-symmetry environments. This species accounts for the sharp feature at g = 4.3. Likewise, the $\mathbf{1}^{red}$ spectrum (Figure S4 in the SI) has contributions from major (88%) and minor (12%) $S = {}^{5}/_{2}$ species with spin-Hamiltonian parameters nearly identical with their $\mathbf{2}^{red}$ counterparts. For both species, we propose that the major $S = {}^{5}/_{2}$ signal corresponds to $\mathbf{X}^{red}$, while the minor signal is attributed to ferric impurities generated from trace amounts of O_2. The EPR results therefore suggest that the putative *p*$SQ^{\bullet}$ ligand is ferromagnetically coupled to the high-spin Fe^{II} center.

Because we were unable to grow X-ray-quality crystals of $\mathbf{1}^{red}$ and $\mathbf{2}^{red}$, structural models of the reduced species with $S = {}^{5}/_{2}$ were derived from DFT calculations; Table S3 in the SI

dx.doi.org/10.1021/ic502564r | Inorg. Chem. 2014, 53, 12240−12242

compares the metric parameters for the $\mathbf{1}/\mathbf{1}^{red}$ and $\mathbf{2}/\mathbf{2}^{red}$ pairs of geometry-optimized models. One-electron reduction of **1** to $\mathbf{1}^{red}$ causes the O2−C4 and O1−C1 bonds to elongate by 0.049 and 0.033 Å, respectively. In addition, the quinoidal character of the ligand is diminished because of lengthening of the C2−C3 bond (by 0.037 Å) and comparable shortening of the C1−C2 and C3−C4 bonds. Similar differences in the ligand bond lengths are observed for the $\mathbf{2}/\mathbf{2}^{red}$ pair (Table S3 in the SI). Such dramatic changes in the O−C and C−C bond distances upon conversion of $\mathbf{X} \rightarrow \mathbf{X}^{red}$ are indicative of a change in the ligand oxidation state from a closed-shell quinone to a semiquinone radical.[13] This conclusion is further supported by the Mulliken spin populations of the iron center (3.78) and the $^{H}\mathbf{J}$ ligand (1.20) in the $\mathbf{1}^{red}$ model.

In agreement with the EPR data, broken-symmetry (BS) calculations found that the iron- and ligand-based spins are ferromagnetically coupled, with computed J values of ∼65 cm^{-1} ($H = -2JS_A \cdot S_B$). Moreover, absorption spectra computed using TD-DFT nicely reproduce key features of the experimental spectra (Figure S5 in the SI); in particular, the calculations predict that each $\mathbf{X}^{red}$ model will display two *p*SQ-based $\pi \rightarrow \pi^*$ transitions in the near-UV region, resulting in an intense absorption band with λ_{max} near 410 nm. The computed spectra also exhibit a moderate $Fe^{II} \rightarrow$ *p*$SQ^{\bullet}$ MLCT band at 530 nm ($\mathbf{1}^{red}$) or 645 nm ($\mathbf{2}^{red}$).

Direct evidence for the presence of a semiquinonate ligand in the $\mathbf{X}^{red}$ complexes was provided by rR studies. The rR spectrum of $\mathbf{1}^{red}$ (Figure 5) displays an intense peak at 1392

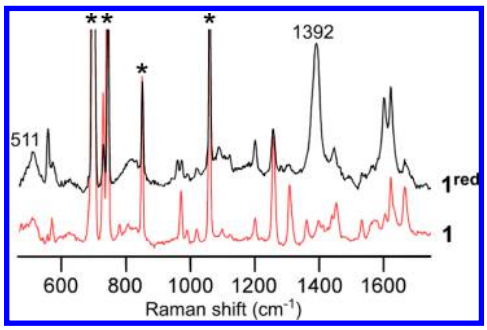

Figure 5. rR spectra obtained with 413.1 nm excitation (40 mW) of $\mathbf{1}^{red}$ (black) and **1** (red) in frozen CD_2Cl_2 solutions. Peaks with an asterisk (*) arise from solvent.

cm^{-1} that is not evident in the precursor spectrum; $\mathbf{2}^{red}$ exhibits a similar feature at 1382 cm^{-1} (Figure S6 in the SI). Both peaks are strongly enhanced by excitation into the near-UV absorption bands. Coordinated SQ radicals typically display an intense peak in the 1400−1500 cm^{-1} region that arises primarily from stretching motions of the C−O bonds.[6e,14] While the observed $\mathbf{X}^{red}$ frequencies fall slightly below this range, the C−O bonds of the semiquinonate ring are likely weakened by charge donation from the phenolate moiety of the $^{R}\mathbf{J}^{2-}$ ligand. This conclusion is supported by DFT frequency calculations with the $\mathbf{1}^{red}$ model, which predict a mode at 1407 cm^{-1} with mixed ν(O−C) and ring-breathing character.

In summary, two mononuclear iron(II) complexes (**1** and **2**) featuring juglone-derived ligands have been prepared and examined with crystallographic and electrochemical methods. Treatment with strong one-electron reductants gives rise to species $\mathbf{X}^{red}$, with coordinated *p*SQ radicals ferromagnetically coupled to high-spin ferrous centers. Current efforts are focused on the preparation of species with greater distances between the iron- and ligand-based spins, thus permitting studies of long-range Fe^{II}−$SQ^{\bullet}$ interactions like those found in PSII.

■ ASSOCIATED CONTENT

Supporting Information

Experimental and computational details, CIF files, Tables S1−S3, and Figures S1−S7. This material is available free of charge via the Internet at http://pubs.acs.org.

■ AUTHOR INFORMATION

Corresponding Author

*E-mail: adam.fiedler@marquette.edu.

Notes

The authors declare no competing financial interest.

■ ACKNOWLEDGMENTS

We thank Dr. Brian Bennett at the National Biomedical EPR Centre (supported by NIH Grant EB001980) and Thomas Brunold (University of Wisconsin) for access to EPR and rR instrumentation, respectively. This research is funded by the U.S. National Science Foundation (Grant CHE-1056845). A.E.B. is supported by an Eisch Research Fellowship.

■ REFERENCES

(1) (a) Yagi, T.; Matsuno-Yagi, A. *Biochemistry* **2003**, *42*, 2266−2274. (b) Cape, J. L.; Bowman, M. K.; Kramer, D. M. *Proc. Natl. Acad. Sci. U.S.A.* **2007**, *104*, 7887−7892. (c) Saito, K.; Rutherford, A. W.; Ishikita, H. *Proc. Natl. Acad. Sci. U.S.A.* **2013**, *110*, 954−959. (d) Mueh, F.; Gloeckner, C.; Hellmich, J.; Zouni, A. *Biochim. Biophys. Acta, Bioenerg.* **2012**, *1817*, 44−65. (e) Klinman, J. P.; Bonnot, F. *Chem. Rev.* **2014**, *114*, 4343−4365.

(2) Xia, D.; Esser, L.; Tang, W.-K.; Zhou, F.; Zhou, Y.; Yu, L.; Yu, C.-A. *Biochim. Biophys. Acta, Bioenerg.* **2013**, *1827*, 1278−1294.

(3) Sarewicz, M.; Dutka, M.; Pintscher, S.; Osyczka, A. *Biochemistry* **2013**, *52*, 6388−6395.

(4) (a) Sedoud, A.; Cox, N.; Sugiura, M.; Lubitz, W.; Boussac, A.; Rutherford, A. W. *Biochemistry* **2011**, *50*, 6012−6021. (b) Nugent, J. H.; Doetschman, D. C.; Maclachlan, D. J. *Biochemistry* **1992**, *31*, 2935−2941.

(5) Machonkin, T. E.; Doerner, A. E. *Biochemistry* **2011**, *50*, 8899−8913.

(6) (a) Garge, P.; Chikate, R.; Padhye, S.; Savariault, J. M.; De Loth, P.; Tuchagues, J. P. *Inorg. Chem.* **1990**, *29*, 3315−3320. (b) Min, K. S.; DiPasquale, A. G.; Golen, J. A.; Rheingold, A. L.; Miller, J. S. *J. Am. Chem. Soc.* **2007**, *129*, 2360−2368. (c) Min, K. S.; Swierczek, K.; DiPasquale, A. G.; Rheingold, A. L.; Reiff, W. M.; Arif, A. M.; Miller, J. S. *Chem. Commun.* **2008**, 317−319. (d) Min, K. S.; DiPasquale, A. G.; Rheingold, A. L.; White, H. S.; Miller, J. S. *J. Am. Chem. Soc.* **2009**, *131*, 6229−6236. (e) Baum, A. E.; Lindeman, S. V.; Fiedler, A. T. *Chem. Commun.* **2013**, *49*, 6531−6533.

(7) Wang, P.; Yap, G. P. A.; Riordan, C. G. *Chem. Commun.* **2014**, *50*, 5871−5873.

(8) Addison, A. W.; Rao, T. N.; Reedijk, J.; Vanrijn, J.; Verschoor, G. C. *J. Chem. Soc., Dalton Trans.* **1984**, 1349−1356.

(9) Baum, A. E.; Park, H.; Wang, D. N.; Lindeman, S. V.; Fiedler, A. T. *Dalton Trans.* **2012**, *41*, 12244−12253.

(10) Sasaki, K.; Kashimura, T.; Ohura, M.; Ohsaki, Y.; Ohta, N. *J. Electrochem. Soc.* **1990**, *137*, 2437−2443.

(11) Connelly, N. G.; Geiger, W. E. *Chem. Rev.* **1996**, *96*, 877−910.

(12) Amada, I.; Yamaji, M.; Sase, M.; Shizuka, H. *J. Chem. Soc., Faraday Trans.* **1995**, *91*, 2751−2759.

(13) Brown, S. N. *Inorg. Chem.* **2012**, *51*, 1251−1260.

(14) (a) Zhao, X.; Ogura, T.; Okamura, M.; Kitagawa, T. *J. Am. Chem. Soc.* **1997**, *119*, 5263−5264. (b) Vlcek, A. *Comments Inorg. Chem.* **1994**, *16*, 207−228.